

Development of a 4D numerical chest phantom with customizable breathing

Pierre-Emmanuel LENI^a, Rémy LAURENT^a, Michel SALOMON^b, Régine GSCHWIND^a, Libor MAKOVICKA^a, Julien HENRIET^a

^a*Informatics and Radiation physics for Medical Applications Team, C.E. Laboratory, UMR CNRS 6249, University of Bourgogne Franche-Comté, France*

^b*FEMTO-ST Laboratory, UMR CNRS 6174, University of Bourgogne Franche-Comté, France*

Abstract

Respiratory movement information is useful for radiation therapy, and is generally obtained using 4D scanners (4DCT). In the interest of patient safety, reducing the use of 4DCT could be a significant step in reducing radiation exposure, the effects of which are not well documented. The authors propose a customized 4D numerical phantom representing the organ contours. Firstly, breathing movement can be simulated and customized according to the patient's anthroporadiometric data. Using learning sets constituted by 4D scanners, artificial neural networks can be trained to interpolate the lung contours corresponding to an unknown patient, and then to simulate its respiration. Lung movement during the breathing cycle is modeled by predicting the lung contours at any respiratory phases. The interpolation is validated comparing the obtained lung contours with 4DCT via Dice coefficient. Secondly, a preliminary study of cardiac and oesophageal motion is also presented to demonstrate the flexibility of this approach. The application may simulate the position and volume of the lungs, the oesophagus and the heart at every phase of the respiratory cycle with a good accuracy: the validation of the lung modelization gives a Dice index greater than 0.93 with 4DCT over a breath cycle.

Keywords: Artificial Neural Network, Radiation Physics, Phantoms, Breath Simulation

1. Introduction

The ICRP (International Commission on Radiological Protection) phantoms are continuously evolving and being refined through research. Indeed, various mathematical phantoms, such as MIRD [1], have been used since 1969. Nevertheless, they were hermaphrodite and nothing existed for children. Therefore, new phantoms appeared, [2, 3], refining the organ representation. Nowadays, the ICRP uses voxelized phantom references based on computed tomography images [4], to resemble as closely as possible, the shapes, volumes and weights of various organs.

Email address: pierre_emmanuel.leni@univ-fcomte.fr (Pierre-Emmanuel LENI)

In parallel to ongoing research regarding phantoms, respiratory movement is also a growing research topic. In 2005, Low *et al.* estimated respiratory movement using a 5-dimension modelization representing object coordinates, current volume and airflow [5, 6, 7]. Other models also exist: in 2010, Eom *et al.* [8] developed a simulation based on the pressure-volume relationship linked to a finite element analysis; Vandemeulebroucke *et al.* [9, 10] introduced the PoPi model, which relies heavily and *a priori* about the movement, since it is built using a 4DCT of the patient. The motion estimation is computed by comparing the images obtained at each respiratory phase with a simulated sequence (built using the spatial registration of images correlated with a cyclic model of breathing). It is also possible to simulate, almost in real time, respiratory movement customized to every patient, using neural networks [11]; and to use external surrogate monitoring to drive a tumor movement model ([12]). Consequently, phantoms tend to take motion into account to obtain a simulation both accurate and as close as possible to physiologic reality. Segars integrated a module for cardiac deformation into his NCAT model [13, 14]. Furthermore, respiratory simulation was implemented, but remains quite limited: it mainly consists in lung deformations and translation/rotation of other organs, such as the liver and kidneys. Respiratory simulation also exists in the XCAT phantom, which relies mainly on lung deformation. This deformation is parametrized using two curves, which offers high flexibility but requires an expert to adapt it for a given patient [15].

Respiratory movement is useful for radiation treatment: a customized breathing phantom associated with patient monitoring during a treatment session allows for detailed monitoring of received doses and could lead to treatment adjustment. Nevertheless, from a radiation protection point of view, 4DCT provides movement information at the cost of increasing patient exposure to radiation (around 30 times the annual natural exposure). Moreover, due to technical limitations, the data may be inaccurate and contain artifacts (classification problem for example). In this context, using a customized simulation for breathing offers advantages for both radiation protection, by limiting the use of 4DCT that could be a significant step in avoiding small doses, whose effects are still not well documented; and for radiation treatment, by providing movement information for more accurate treatment planning as well as monitoring the dose actually delivered during a treatment session via the breathing cycle recorded from the patient.

Using Artificial Neural Networks (ANN), we proposed two methods: for the simulation of pulmonary movement [11], and for the adaptation of the IRSN (French radiation protection and nuclear safety institute) phantoms [16, 17]. These two projects aim at developing adapted tools for a customized and accurate modelization of the human body, either in a radiation protection context (anthroporadiometry), or for delivering external beam treatment more accurately. In radiation therapy, ANN has recently been used to simulate the tumor movement according to external position trackers [18].

In this paper, our contribution includes a new customized phantom model that simulates realistic respiratory motion of the lungs. The breathing cycle is simulated and validated using 4DCT data. The Dice indices are computed for every respiratory phase section 3. We also present some preliminary results for

simulations of cardiac and oesophageal motion (section 4).

2. Method: ANN presentation

2.1. The neural network

The NEMOSIS (NEural NETwork MOtion SIMulation System) platform has been presented and validated in previous work [11]: using an artificial neural network, it is possible to simulate pulmonary movement customized per patient. Nevertheless, customization was limited by a small amount of patient data, resulting in small learning sets. Moreover, only the internal anatomic structure of the lungs was considered. In this platform, a multi-layer perceptron with one hidden layer is trained using supervised learning. The synaptic weights and biases are optimized to minimize the mean squared error (MSE) using the gradient based Limited-memory Broyden-Fletcher-Goldfarb-Shanno method (L-BFGS) [19] combined with the Wolfe linear search [20] to determine the optimal step size. Moreover, 1000 iterations are performed beyond the minimum MSE to prevent overfitting by checking that a degradation is observed on the interpolation of the generalization set. An incremental approach determines the optimal number of neurons in the hidden layer [21]. The application of NEMOSIS to anthropomorphic phantoms requires several adjustments:

- Adding more patient data to the learning set via collaboration with Besançon CHRU,
- Adding the overall lung contours to the data (for 8 patients over 16),
- Modification of the ANN to improve the customization and compatibility with the IRSN phantoms : find relevant characteristics of the lung to be used as ANN entries.

The IRSN phantoms were generated by proportionally adapting an initial model for various heights [22, 23]. Nevertheless, the analysis and the comparison between patient data and the phantoms demonstrated differences between real and theoretical morphologies. To represent the size of the lungs in the Superior-Inferior axis (SI axis), we take into account the size of the right lung (which is independent of the heart). The measures on the Anterior-Posterior axis and Left-Right axis (AP and LR axes) are performed along the axial plane of the carina to allow reproducibility in all patients and phantoms. Using these two axes, we have approximated the lung bounding box by using a cylinder generated by an ellipse. The ellipse perimeter P ($P = \Pi\sqrt{2((\frac{d_{AP}}{2})^2 + (\frac{d_{LR}}{2})^2)}$) is presented in the last column of the tables 1 and 2. This bounding box is used as an ANN entry.

Tables 1 and 2 are sorted according to pulmonary volume. Table 1 shows that there is no correlation between patient height and lung volume. For example, a person measuring around 1.65 meters can have a pulmonary volume of 2.53 liters (163 cm) or 4.15 liters (165 cm). Similarly, the size of the lungs along the vertical axis (*i.e.* SI axis) is not a linear function of height. Nevertheless, pulmonary volume can be

Height	Age/Gender	Pulmonary volume (liter)	Right lung dimension	LR Axis dimension	AP Axis dimension	Representative ellipse perimeter
1620	88/F	2.53	185	224.90	149.30	599.67
1630	-/F	2.60	190	204.10	148.44	560.63
1700	83/M	3.11	185	248.05	166.99	664.26
1680	74/M	3.71	227.5	230.90	148.10	609.37
1540	73/F	3.85	240	208.99	157.27	580.97
1660	77/M	4.04	200	244.14	185.55	681.20
1800	64/M	4.05	220	244.14	161.13	649.81
1650	78/M	4.15	247.5	226.85	166.88	625.60
1740	-/M	4.42	220	221.20	195.68	656.06

Table 1: Measures (in mm) of the lungs for various patients, obtained from computed tomography images, besides the perimeters, computed using the measures along the AP and LR axes.

Height	Pulmonary volume (liter)	Right lung dimension	LR Axis dimension	AP Axis dimension	Representative ellipse perimeter
1650	2.64	224.82	208.07	118.14	531.52
1680.3	2.81	229.46	212.36	120.58	542.49
1731.8	3.10	236.92	219.26	124.50	560.12
1758	3.24	240.54	222.62	126.40	568.69
1783.1	3.38	243.91	225.74	128.17	576.66
1807.1	3.51	247.08	228.67	129.84	584.15
1850	3.75	252.50	233.68	132.68	596.94

Table 2: Measures (in mm) of the lungs for the IRSN female phantoms, obtained through mesh measurements, besides the perimeters.

represented by the volume of the aforementioned cylinder. The ANN concept is extensively described in the literature [24]. The entries of the ANN are raw data to avoid biasing the learning. Therefore, the existing entries (3D coordinates of a point (its location along the 3 axis X , Y and Z), pulmonary volume, and respiratory phase) have been complemented by three new ones, which represent an approximation of the real pulmonary volume by a cylinder, *i.e.* the dimensions along the SI, AP and LR axes. Unfortunately, we note that the dimensions along the AP axis for all the phantoms are inferior to the patient's. As already stated [11], NEMOSIS is an interpolator *inside* the definition domain of the training data. Since the learning step is performed using patient data, the dimensions along the AP axis cannot be used for simulation on the phantoms. Therefore, the entries using the dimensions along AP and LR axes are replaced by the perimeter.

Moreover, the perimeter is correlated with chest size and thus can be "externally" measured. Only phantoms with a height greater than 173.18 cm are included in the definition domain; thus, further studies are limited to these phantoms. Ultimately, 7 variables constituted the entries of the NEMOSIS ANN:

- 3D point coordinates,
- Pulmonary volume,
- The cylinder perimeter,
- The dimension of the right lung (*i.e.* the cylinder height), and
- The respiratory phase.

In other words, given the external measurement of a person and the desired respiratory phase, the network can simulate the corresponding customized lung contours.

2.2. The training data

The learning set for pulmonary movement was constituted by 4DCT images of 15 patients acquired during free breathing and sorted into 5 phases by the 4DCT. Firstly, on every 4DCT, positions of anatomic points are manually defined by experts and tracked over various respiratory phases, for a total of 4680 points (10 phases per patient). These points are internal characteristic locations within the lungs that are recognizable over the phases (*e.g.* vessels, bronchus unusual junctions). Since the IRSN phantoms consist of the organ contours only, an algorithm (region-growing) has been implemented to automatically extract the lung contours of the patients on every 4DCT. Indeed, there is no visual reference to identify a point over phases, so we take advantage of parametric curves:

- Every lung has 4 ridge lines (top and bottom most points along the LR and AP axis),
- A ridge line is a spline (a parametric curve). The control points of the splines are the extreme points of the lungs on every section,
- An identical parameter value over time defines the same point over different phases.

90 to 115 points per ridge line are computed, which leads to 720 to 920 contour points per patient. A total of 3248 points per phase are added to the dataset, which leads to 37160 points for 15 patients over 10 phases, including the anatomic points.

The Figure 1 illustrates the spline interpolation (in red) of the lung contours. For any number of points guiding the spline, a position along the curve can be defined by a parameter (a real value) varying between 0 and 1. In this example, three points (in yellow) are drawn, corresponding to the parameterization values 0.5, 0.7 and 0.8 (chosen for illustration purpose). We can observe that these locations can be represented

at every phase, by using the same parameter value, even if the spline is not defined by the same number of points.

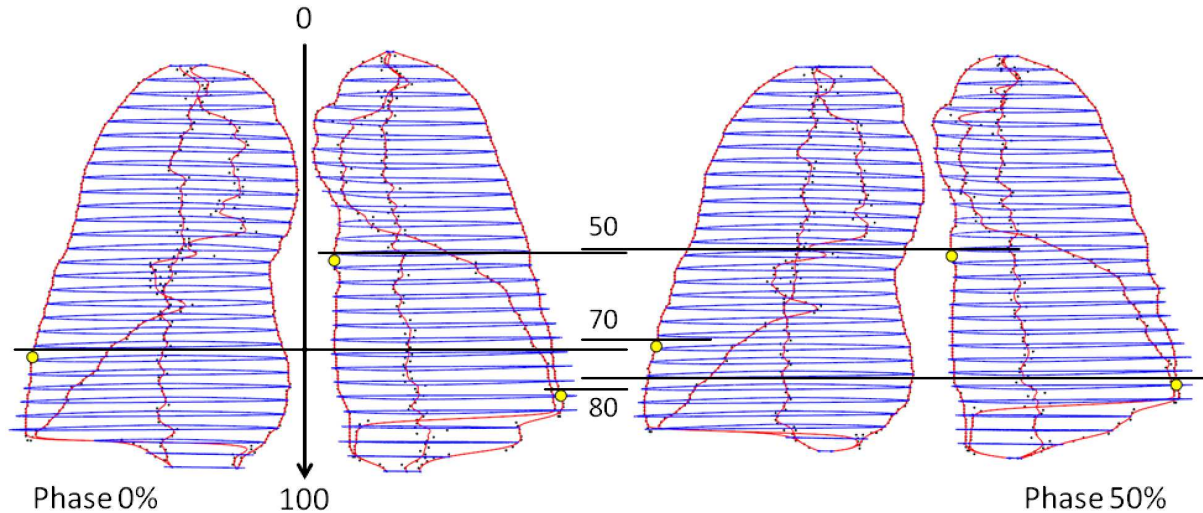


Figure 1: Spline interpolation of the lung contours.

The automatic incrementation algorithm of the number of neurons presented in [11] is used. The dataset is split into two sets: a learning set and a generalization set. The generalization set is used to check the ANN interpolation performances during the learning step, to prevent over-fitting, and to stop the process when it starts diverging from the best solution. The results presented in the following section correspond to the best results : the learning set contains 12 patients, and the generalization set contains 3 patients. 20 neurons between the entries and the output layer have been determined as the best topology by the learning algorithm. Various constructions of the learning and generalization sets have been tested for the ideal data division.

3. Results: Lung movement and validation

3.1. Simulated movement

The number of phases to simulate can be adjusted. Two configurations are considered: 10 phases and 100 phases. To emphasize the movement gradients, we present the results obtained for 10 phases. 100 phases may allow the simulation of any lung movement (such as a sigh) or irregular breathing. Table 3 presents the simulation of respiratory movement using NEMOSIS on IRSN phantoms. The two phantoms represented are at the boundary of the definition domain (cylinder perimeter). The maximum exhalation point, *i.e.* the minimum pulmonary volume, is reached between the 50 to 60% respiratory phases. The variation between the various 4D TDM are due to the acquisition uncertainties and synchronization with the breath signal.

NEMOSIS computes the minimum at the phase 60% when 10 phases are simulated (as in Table 3), and 53% when 100 phases are generated.

HeightPhantom volume (cm)	$ANN_{0\%}$ volume (l)	$ANN_{60\%}$ volume (l)	$\Delta Vol_{Phant-ANN}$ (l)	$\Delta Vol_{60\%-0\%}$ (l)
175.8	3.240	3.235	0.005	0.138
185	3.747	3.725	0.022	0.185

Table 3: NEMOSIS applied on 2 phantoms at the boundary of the definition domain. The measured are performed at two respiratory phases: 0% and 60%, the minimum and maximum lung volumes, respectively. The Δ measures represent the difference between the phantom and the RNA, and between the phases 60% and 0%.

Figure 2 presents the breath simulation obtained for the 185 cm phantom using NEMOSIS. The phantom is rendered at 5 respiratory phases (10, 30, 50, 70 and 90%). Since the number of points within the contour is constant, a color code is used to demonstrate the amplitude of movement of a point from its current position to its position at the next phase. The initial lung contour (phase 0%) is represented on every phase to visualize the global movement amplitude. In this case, the maximum magnitude is 12.54 mm. The mean and standard deviations are computed for all the point variations at every phase. The main direction of the movement gradient is along the SI axis, which corresponds to reality. Indeed, despite the numerous muscles involved in respiration (intercostals, scalenes, diaphragm), the main one is the diaphragm. Its contraction deforms the lungs, including their contour as well as their internal anatomy.

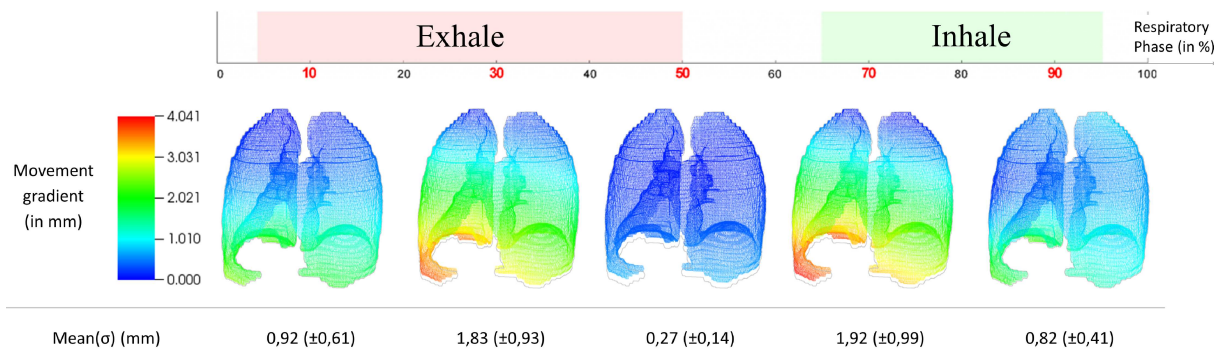


Figure 2: Simulation of the lung movement using NEMOSIS on the 185 cm phantom.

3.2. Validation

Validation is conducted by comparing ANN simulations with the 4DCT images of 3 patients, phase by phase. The patients had lung dimensions and contour coordinates included in the learning set minimum and maximum values. These data were not used during the training step.

Table 4 shows the pulmonary volumes computed using the simulated contours on the test patients. In this case, since the number of points is not the same for every phase, it is not possible to compute the error per point. Instead, the volumes are compared using the Dice index, which evaluates the similarity between two sets (see equation 1, V_{4D} and V_{NEM} representing the measured volume on 4DCT and simulated using NEMOSIS, respectively). Unfortunately, some 4DCT were not available for some phases so the corresponding comparisons were not computed.

$$D(V_{4D}, V_{NEM}) = \frac{(2card(V_{4D} \cap V_{NEM}))}{(card(V_{4D}) + card(V_{NEM}))} \quad (1)$$

		Phase (%)									
		0	10	20	30	40	50	60	70	80	90
Patient A	$V_{4D}(l)$	5.69	5.64	5.54	5.44	5.32	5.22	5.19	5.28	5.43	5.57
	$V_{NEM}(l)$	5.68	5.63	5.61	5.50	5.45	5.40	5.42	5.49	5.58	5.67
	$V_{4D} \cap V_{NEM}(l)$	5.68	5.53	5.43	5.30	5.20	5.15	5.01	5.21	5.39	5.54
	$D(V_{4D}, V_{NEM})$	1.000	0.981	0.974	0.969	0.966	0.970	0.944	0.967	0.979	0.986
Patient B	$V_{4D}(l)$		5.01	4.99		4.93		4.87		4.96	
	$V_{NEM}(l)$		5.17	4.96		4.81		4.56		4.76	
	$V_{4D} \cap V_{NEM}(l)$		4.96	4.77		4.64		4.47		4.62	
	$D(V_{4D}, V_{NEM})$		0.966	0.959		0.953		0.948		0.951	
Patient C	$V_{4D}(l)$			4.24		4.13		4.10	4.11		4.16
	$V_{NEM}(l)$			4.26		4.19		4.24	4.24		4.37
	$V_{4D} \cap V_{NEM}(l)$			4.05		3.90		3.90	3.92		4.03
	$D(V_{4D}, V_{NEM})$			0.955		0.937		0.935	0.939		0.946

Table 4: Simulation of the lung movements on the test patients.

The Figure 3 illustrates lung contours for patient A extracted from 4DCT data at the 70% respiratory phase, and the corresponding contours simulated by NEMOSIS. We note that the contours are not distorted. On this example, the Dice index is equal to 0.97.

4. Discussion: limits of current approach and extension to other organs

4.1. Simulated lung movement

We propose an ANN-based approach to simulate the organ contour at any respiratory phase. Our solution has been tested on both phantoms, and it can be noted that NEMOSIS simulates the largest variations during the breathing cycle for the tallest phantom. This behavior is related to the phantoms:

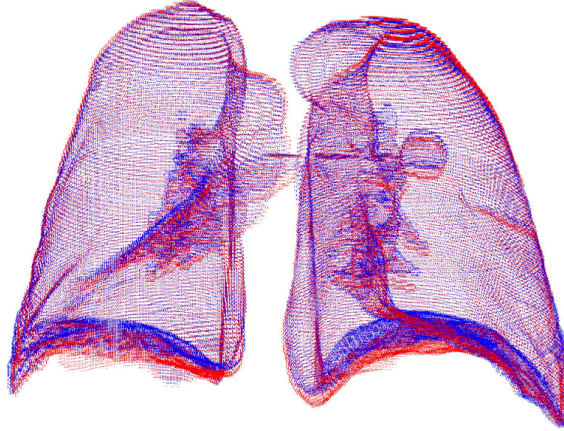


Figure 3: Comparison between 4DCT data (in blue) and NEMOSIS (in red) at the phase 70%.

they are generated from a model by applying a proportionality coefficient along the 3 dimensions, without any morphologic difference. To validate the approach, we compare the ANN results with 4DCT data using Dice index. Table 4 shows that for patient A, the maximum exhalation point is obtained at 53% using NEMOSIS, but measured on the real patient at 60%: while the real patient is still inhaling, the simulation has already started exhaling. Thus, for the phases 60% to 90%, NEMOSIS is "in advance" and provides higher volumes than reality. Despite this, the correlation between NEMOSIS and reality is very promising, providing a Dice index higher than 0.94. By construction, the ANN can only perform the interpolation for the input data included inside the learning set. For example, if the patient heights for training are between 160cm and 165cm, to be able to use ANN for a 170cm person, the learning sets has to be extended.

4.2. Cardiac and Oesophageal movement

Only three 4DCT are currently available with heart and oesophageal information. Moreover, these data are incomplete, with missing phases and/or incoherent data. Indeed, these organ contours are manually defined. Nevertheless, since the data are acquired using breath synchronization (and thus 10 phases), the main movement measured on the heart and oesophagus is likely due to the breathing and lung deformation. Therefore, for a preliminary study, we simulate the movement of both organs using the ANN used for lungs. Although it is not an ANN dedicated to these organs, the training using the lungs allows for presenting interesting results, but requires further improvements. It certainly illustrates the feasibility and flexibility of our approach. To compare the movement simulated by NEMOSIS with the 4DCT data, only the sections (*i.e.* CT images along the SI axis) having mutual contour definitions are retained. Table 5 presents the oesophagus and the heart dice index, between the simulated volumes using NEMOSIS and the 4DCT data.

The Dice indices of patient 2 (around 0.8) and of patient 1 (greater than 0.82) are encouraging: even at the phases with large movement gradients, the simulated position of the oesophagus is correct, provided that the contour definitions (on 4DCT) are consistent over all phases. The Dice index of patient 3 is lower than 0.75, due to poor contour definition on the 4DCT.

$D(V_{4D}, V_{NEM})$		Phase (%)									
		0	10	20	30	40	50	60	70	80	90
Patient 1	for oesophagus	1.000		0.859	0.838		0.820	0.826	0.849		0.848
	for heart	1.000		0.939	0.917	0.912	0.905	0.902	0.926		0.919
Patient 2	for oesophagus	1.000	0.801	0.777		0.800	0.803	0.710			
	for heart	1.000	0.946	0.943	0.933	0.934	0.943	0.942			
Patient 3	for oesophagus	1.000	0.730	0.741	0.708	0.677	0.643	0.602	0.683	0.759	
	for heart	1.000	0.960	0.954	0.955		0.942	0.952	0.951	0.938	

Table 5: Simulation of the oesophagus and heart movement using NEMOSIS.

Figure 4 illustrates these results for the patient 1 in the worst case. All the sections available either through ANN or 4D are represented. We can notice that the shape is preserved, and the anatomic characteristics (such as the curvature at the bottom) are properly located.



Figure 4: Comparison of patient 1 oesophageal shape at the 50% phase. In black: expert's contour definition, in blue: NEMOSIS contours.

5. Conclusions and perspectives

We have presented an approach to reproducing breath movement on 3D phantoms. Our contribution consists of the training of ANN, the NEMOSIS application, to simulate the position and volume of the lungs, the oesophagus and the heart at every phase of the respiratory cycle. The ANN are trained using organ contours extracted from 4DCT acquisitions of real patients. The interpolation of the lung contours is validated by comparing the ANN results with 4DCT, on 3 patients, not used during network training. The Dice index is used to measure the superposition of interpolated and 4DCT lung contours, and the obtained results (Dice indices greater than 0.94) show the accuracy of the simulation. The aim of this approach is to improve the patient radiation protection by limiting the 4DCT acquisitions, which could be substituted or sustained by respiratory simulation from one 3DCT acquisition.

Nevertheless, the results presented for the heart and the oesophagus cannot yet be validated using the same approach, and adding new data for cardiac and oesophageal motion is a priority. Moreover, when enough data is available, one ANN will be trained for every organ (3 in total). Therefore, it is important to ensure that no superpositions nor collisions exist between the interpolated organ contours. Several solutions may be considered, such as working directly with voxel data. Finally, other movements should be taken into account, such as the heart beat and swallowing, which is complex: 4D TDM are synchronized with breathing but these other movements cannot be acquired using this tool.

6. Acknowledgements

The authors would like to thank the Besançon university hospital (CHRU) for providing patient data. These works were supported by a funding obtained during a call for projects in the INSERM's PhysiCancer plan, which we would like to sincerely thank. Finally, the authors would like to thank the reviewers for their constructive remarks, and Dr. G. Hruby (Staff specialist, Sidney) for carefully reading this article.

- [1] Snyder WS, Ford MR, Warner GG, Watson BB. Medical internal radiation dose committee (MIRD) pamphlet no. 5 (1969). *J Nucl Med.* 1969;10.
- [2] Kramer R, Zankl M, Williams G, Drexler G. The calculation of dose from external photon exposures using reference human phantoms and Monte Carlo methods, Part I: The male (Adam) and female (Eva) adult mathematical phantoms. GSF-Centre national de recherche en environnement et santé, Neuherberg, Allemagne.; 1982. GSF S-885.
- [3] Cristy M, Eckerman KF. Specific Absorbed Fractions of Energy at Various Ages from Internal Photon Sources: 1, Methods. Atomic Energy Research Establishment.; 1987.
- [4] Menzel HG, Clement C, DeLuca P. ICRP Publication 110. Adult reference computational phantoms. *Annals of the ICRP.* 2009;39(2):1.
- [5] Low DA, Parikh PJ, Lu W, Dempsey JF, Wahab SH, Hubenschmidt JP, et al. Novel breathing motion model for radiotherapy. *International Journal of Radiation Oncology*Biophysics*Physics.* 2005;63(3):921–929.
- [6] Yang D, Lu W, Low DA, Deasy JO, Hope AJ, Naqa IE. 4D-CT motion estimation using deformable image registration and 5D respiratory motion modeling. *Medical physics.* 2008;35:4577.

- [7] Zhao T, Lu W, Yang D, Mutic S, Noel CE, Parikh PJ, et al. Characterization of free breathing patterns with 5D lung motion model. *Medical physics*. 2009;36:5183.
- [8] Eom J, Xu XG, De S, Shi C. Predictive modeling of lung motion over the entire respiratory cycle using measured pressure-volume data, 4DCT images, and finite-element analysis. *Medical physics*. 2010;37:4389.
- [9] Vandemeulebroucke J, Sarrut D, Clarysse P, et al. The POPI-model, a point-validated pixel-based breathing thorax model. In: *XVth international conference on the use of computers in radiation therapy (ICCR)*. vol. 2. Citeseer; 2007. p. 195–199.
- [10] Vandemeulebroucke J, Rit S, Kybic J, Clarysse P, Sarrut D. Spatiotemporal motion estimation for respiratory-correlated imaging of the lungs. *Medical physics*. 2011;38:166.
- [11] Laurent R, Henriët J, Salomon M, Sauget M, Gschwind R, Makovicka L. Respiratory lung motion using an artificial neural network. *Neural Computing and Applications*. 2012;21(5):929–934.
- [12] Martin J, McClelland J, Yip C, Thomas C, Hartill C, Ahmad S, et al. Building motion models of lung tumours from cone-beam CT for radiotherapy applications. *Physics in medicine and biology*. 2013;58(6):1809.
- [13] Segars WP, Lalush DS, Tsui B. Modeling respiratory mechanics in the MCAT and spline-based MCAT phantoms. *Nuclear Science, IEEE Transactions on*. 2001;48(1):89–97.
- [14] Segars WP, Tsui BM, Lalush DS, Frey EC, King MA, Manocha D. Development and application of the new dynamic Nurbs-based Cardiac-Torso (NCAT) phantom. The University of North Carolina; 2001.
- [15] Segars WP, Sturgeon G, Mendonca S, Grimes J, Tsui B. 4D XCAT phantom for multimodality imaging research. *Medical physics*. 2010;37:4902.
- [16] Farah J, Henriët J, Broggio D, Laurent R, Fontaine E, Chebel-Morello B, et al. Development of a new CBR-based platform for human contamination emergency situations. *Radiation protection dosimetry*. 2011;144(1-4):564–570.
- [17] Henriët J, Chebel-Morello B, Salomon M, Farah J, Laurent R, Sauget M, et al. EquiVox: an example of adaptation using an artificial neural network on a case-based reasoning platform. *Biomedical Engineering: Applications, Basis and Communications*. 2013;25(02):1350027.
- [18] Seregni M, Pella A, Riboldi M, Orecchia R, Cerveri P, Baroni G. Real-time tumor tracking with an artificial neural networks-based method: a feasibility study. *Physica Medica*. 2013;29(1):48–59.
- [19] Hsieh WW. *Machine learning methods in the environmental sciences: neural networks and kernels*. Cambridge university press; 2009.
- [20] Nocedal J, Wright S. *Numerical optimization*. Springer Science & Business Media; 2006.
- [21] Sauget M, Laurent R, Henriët J, Salomon M, Gschwind R, Contassot-Vivier S, et al. Efficient domain decomposition for a neural network learning algorithm, used for the dose evaluation in external radiotherapy. In: *Artificial Neural Networks–ICANN 2010*. Springer; 2010. p. 261–266.
- [22] Clairand I, Bouchet LG, Ricard M, Durigon M, Paola MD, Aubert B. Improvement of internal dose calculations using mathematical models of different adult heights. *Physics in Medicine and Biology*. 2000;45:2771–2785.
- [23] Farah J, Broggio D, Franck D. Examples of Mech and NURBS phantoms to study the morphology effect over in vivo lung counting. *Radiation Protection and Dosimetry Special Issue*. 2011;144:344–348.
- [24] Laurent R. *Simulation du mouvement pulmonaire personnalisé par réseau de neurones artificiels pour la radiothérapie externe*. University of Franche-Comté; 2011.